Synergistic effect of hybrid nanodiamond/ZnO nanowires for improved ultraviolet photoresponse

Jiang Haitao[1,2], Liu Shibin[1], Yuan Qianqian[2]

(1. School of Electronics and Information, Northwestern Polytechnical University, Xi′an 710129, China;
2. Jiao Zuo Teachers College, Jiaozuo 454001, China)

Abstract: ZnO-based photodetectors (PDs) have a small on/off ratio and long response time, which hamper their practical UV detection. Herein, a facile method to prepare a nanodiamond (ND)-decorated ZnO nanowire (ZNW) ultraviolet photodetector was demonstrated. This hybrid ZnO-ND UV photodetector considerably improved photodetection performance compared with bare ZnO. This hybrid device simultaneously exhibited remarkable detectivity, rapid response, and decent current on/off ratio. This excellent performance was attributed to the synergistic effect between NDs and the ZNWs. These results introduce a new scenario for designing and fabricating an innovative optoelectronic system.

Key words: nanodiamond; synergistic effect; nanowire; ultraviolet photodetector

CLC number: TN304.9;O472+4 **Document code:** A **DOI:** 10.3788/IRLA201948.0120004

纳米金刚石和氧化锌纳米线的协同效应提高紫外光电响应

蒋海涛[1,2],刘诗斌[1],元倩倩[2]

(1. 西北工业大学 电子信息学院,陕西 西安 710129; 2. 焦作师范高等专科学校,河南 焦作 454001)

摘 要: 氧化锌基紫外光电探测器较小的开关比和长的响应时间,制约其在紫外检测中的实际应用。一种简易制备纳米金刚石修饰氧化锌纳米线紫外光电探测器的方法,纳米金刚石和氧化锌纳米线混合物光电探测器的光电性能比氧化锌光电探测器有明显的提升:快的响应时间和好的开关比;优异的光电性能得益于纳米金刚石和纳米线之间的协同效应。这种策略为设计和制备新型光电系统提供了一种可能。

关键词: 纳米金刚石; 协同效应; 纳米线; 紫外光电探测器

收稿日期:2018-08-11; **修订日期**:2018-09-17

基金项目:国家自然科学基金(61605207);河南省科技攻关项目基金(182102210419)

作者简介:蒋海涛(1978-),男,副教授,博士,主要从事微电子器件和微传感器方面的研究。Email:jzchaonan@163.com

通讯作者:刘诗斌(1960-),男,教授,博士,主要从事智能传感器系统和微电子器件与微传感器方面的研究。Email:liushibin@nwpu.edu.cn

0 Introduction

Metal oxides are important building blocks for next-generation electronics, including sensing elements[1-6], transparent conductive electrodes [7], energy harvesting and storage devices[8-10], and optoelectronics[11-18]. Among them, ZnO nanostructures, especially ZnO NWs, which bear a large specific surface area, a direct and wide bandgap (~3.37 eV), size-dependent physical properties, rapid charge transport characteristics[19], and high optical absorption in the UV range, are promising candidates for nanoelectronics and nanophotonics[20-22]. Meanwhile, UV photodetection is important for environmental and biological research, space technology, and missile launch [23-24]. UV photodetectors with different detection wavelengths play an important role in radiation warning, flame detection, missile tracking, and encrypted signal transmission[25-29]. ZnO NWs should be facilely fabricated and integrated into UV PDs with high performance and low cost to fulfil their potential in UV photodetection.

A great amount of oxygen molecules is adsorbed onto the ZnO surface to form a low-conductivity depletion layer due to their large surface-to-volume ratio[30-31], which hampers practical UV photodetection. Various strategies have been implemented to enhance the perfor-mance of ZnO-based UV PDs[32-35]. For example, the plasmonic effect effectively improves the photoresponse performance of semiconductor devices[32,36]. The increase time could be drastically reduced from hundreds of seconds to a value less than 1 s by utilizing Schottky contact instead of ohmic contact in ZnO NW PDs[30-31]. In addition, ZnO has been successfully nanoscaled by doping with reinforcement elements[37] and modifying with metal oxides[38-39] and carbon nanotubes[40-41].

However, these strategies involve either surface modification on NWs or special fabrication processes, such as post-growth NW transfer and lithographic processes, which are undesirable for low-cost and large-scale production. In this paper, we report a catalyst-free fabrication of ZnO NWs and a facile post-treatment method by spinning NDs and annealing treatment. The fabricated device demonstrated a robust photocurrent under UV illumination in air at room temperature. We attributed this excellent performance to the synergistic effect between NDs and ZnO NWs. These results introduce a new scenario for designing and fabricating an innovative optoelectronic system.

1 Experimental section

1.1 Fabrication and Characterization of ZnO NWs

The growth of ZnO NWs was investigated in a horizontal tube furnace with a quartz tube vacuum chamber 100 cm in length and 10 cm in diameter. The key step before growing is roughening the surface of SiO_2/Si wafer with mechanical, chemical, or plasma etching. Then, the mixture of the ZnO powder (99.99%) and graphite powder (weight ratio 1:1) was placed in the quartz coat as the precursor material, and the plasma etching treated the SiO_2 side facing the source. High-purity Ar gas, as carrier gas, was first fed into the furnace at the rate of 100 sccm, and the pressure in the quartz tube was adjusted to 30 kPa. When the temperature was heated to the designed temperature, high-purity O_2 gas was introduced into the quartz tube at the rate of 2 sccm. However, the precursor material was heated up to 960 ℃, and the temperature was maintained to approximately 30 min during the growth of the ZnO NWs. When the growth was over, the oxygen was switched off and the furnace was naturally cooled down to room temperature.

The morphology and crystal structure of the ZnO NWs were characterized by high-resolution transmission electron microscopy (TEM, JEM2100), field-emission scanning electron microscopy (SEM, JEOL7600), X-ray diffraction (XRD) (Rigaku RINT2500TRAX-III, Cukα radiation), and X-ray photoelectron spectroscopy (XPS).

1.2 Device fabrication and characterization

In the fabrication process, the SiO_2/Si substrate with ZnO NWs was placed on the spin coater. Then, some drops of ND suspension (Adrich-Sigma) were deposited on the ZnO NWs, rotated at 1 000 rpm for 20 s to achieve uniform ND distribution, and then dried at 140 ℃ for 30 min to vaporize the solvent. Subsequently, the silver paint (CW2400, ITW Chemtronics) was directly applied onto the ZnO-ND NWs to form the electrodes, with an internal space of approximately 4 mm and sufficient thickness.

Photoresponse testing was performed on an electrochemical workstation (CHI 660D). The sampling period was set to 20 s, and the change in the current of the UV photodetector with or without light illumination was recorded by the electrochemical workstation. A 400 W xenon lamp with an output window diameter of 10 cm was adopted as the light source, and the UV power density incident to the device surface was approximately 14 mW/cm. The "on" and "off" switches of the illumination were controlled by a chopper. All measurements were conducted in a darkroom to minimize the influence of natural light.

1.3 Result and discussion

The morphology of the products was investigated by field-emission SEM. Fig.1(a) and (c) show the top view SEM images of the as-grown ZnO NWs and ZnO-NDs, respectively. Fig.1(a) and the corresponding inset show that the diameter of the nanowires is approximately 200 nm. Fig.1 (b) and (d) show the elemental mapping profiles of the ZnO NWs and ZnO-NDs NWs, respectively. In Fig.1 (b), only the Zn, O, and C elements are observed, whereas no other impurities are detected. The morphology of the ZnO NWs coated with NDs in Fig.1(c) and (d) indicates that this architecture is composed of ND particles compactly and uniformly, revealing that the NDs successfully decorated the ZnO nanowires.

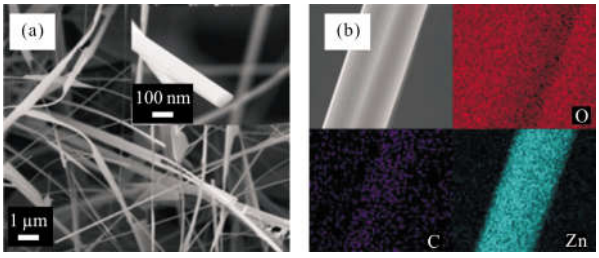

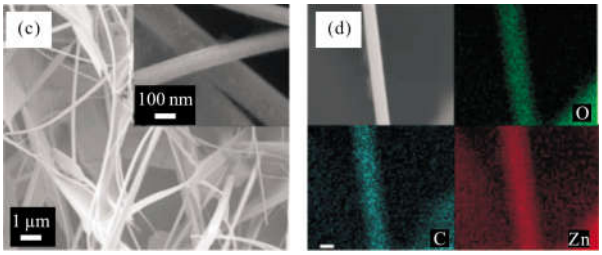

Fig.1 (a) and (c) Top view SEM images of the as-grown ZnO NWs and ZnO-NDs NWs, respectively; the insets are the high resolution of the corresponding samples; (b) and (d) Zn, O, and C element mapping of ZnO NWs and ZnO-NDs, respectively

TEM images are shown in Fig.2 (a) and (c), further confirming the structure of the bare ZnO NWs and ZnO-NDs. The bare ZnO NWs in Fig.2 (a) exhibit clear lattice fringes of ZnO nanowires. The interplanar distance is 0.26 nm, which is in good agreement with the distance spacing of the (0002) lattice plane of a hexagonal ZnO wurtzite structure, further confirming that (0002) is the preferential growth direction of these ZnO NWs. For the ZnO-

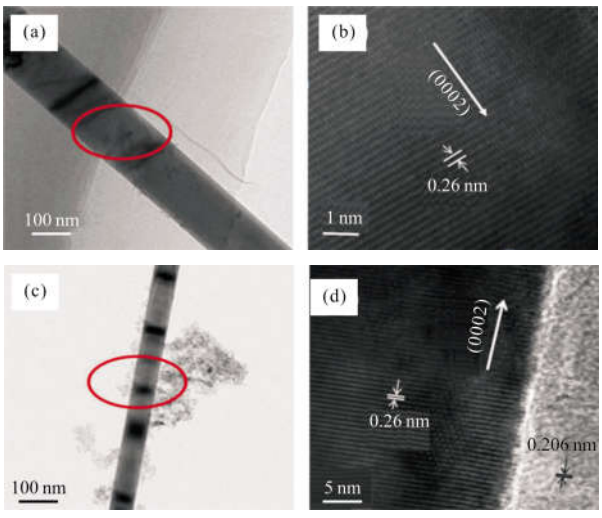

Fig.2 (a) and (c) show the sample of the ZnO NWs and ZnO-NDs NWs used for TEM, respectively; TEM images of ZnO NWs (b) and ZnO-NDs (d)

NDs nanowires, the TEM image reveals two types of lattice fringes from ZnO and NDs. On the ZnO side, the lattice constant is similar to that of the bare one, whereas on the nanoparticle side, the interplanar distance of 0.206 nm corresponds to the distance spacing of the (111) lattice plane of a diamond zinc blended structure.

Crystallographic information was obtained from the XRD pattern of the bare ZnO NWs (Fig.3(a)). The diffraction peaks can be indexed to a hexagonal structure of ZnO, which still maintains the previous crystalline with cell constants of a=3.24 Å and c= 5.2 Å. No impurity peak could be observed from the XRD pattern, contrary to that of ZnO NWs grown by catalyst-assisted CVD methods[42].

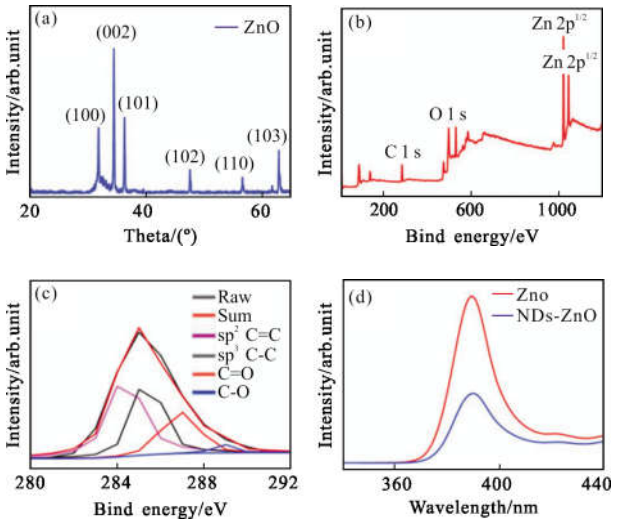

Fig.3 (a) XRD patterns of ZnO NWs; (b) XPS wide survey spectra of ZnO–NDs NWs; (c) C 1s spectra of ZnO–NDs NWs; (d) PL spectrum of the ZnO and ZnO–NDs NWs

To verify the chemical states of C elements in the prepared ZnO–NDs NWs, we performed XPS to analyze the ZnO–ND NW surface state. Fig.3(b) and (c) present the XPS wide survey spectra and C 1 core–level peaks of the ZnO–NDs NWs, respectively. The C 1 peaks (Fig.3 (c)) can be fitted by four Gaussian peaks, namely, sp^2 C=C (284.4 eV), sp^3 C–C (285.4 eV), C–O (286.9 eV), and C=O (288.7 eV), located at ~284.4, ~285.4, ~286.9, and 288.7 eV, respectively[43]. The sp^3 C–C subpeak indicates the apparent transformation of non-diamond to diamond phase, whereas the sp^2 C=C subpeak illustrates the presence of a small sp^2 C fraction on the ZnO–NDs[44]. The C–O and C=O subpeaks reveal that abundant functional groups are detected in ZnO–NDs, especially C–O and C=O. These functional groups on the surface of ZnO–NDs act as photoluminescence (PL) centers[45]. Therefore, PL measurements of ZnO and ZnO–NDs were carried out at room temperature on these two samples. Fig.3(d) shows the PL spectra of the ZnO NWs and ZnO–NDs NWs excited by a Xe lamp at 280 nm. The PL intensity of the ZnO–NDs is much weaker than that of the bare ones, revealing that the recombination of the photoexcited electron-hole pairs in ZnO–NDs has been strongly suppressed. A comparatively weak peak at a similar position is also observed due to a direct transition between the conduction band and a low-lying valence band. Meanwhile, the exciting peak of ZnO–NDs is approximately half of the bear ZnO, indicating that the electron-hole pairs have weaker recombination than the bare ZnO because of a charge transfer process between the contact surface of the NDs and ZnO nanowires.

1.4 Optoelectronic performance of ZnO and ND–ZnO ultraviolet photodetector

Photoresponse tests were conducted in a dark chamber with a UV LED as the light source (365 nm, 14 mW/cm^2). The "on" and "off" switches of illumination were controlled by a mechanical chopper. The photoresponse of the ZnO NW array-based and ZnO–NDs NW–based PDs to UV illumination is shown in Fig.4. Fig.4(a) shows the asymmetrical I–V curves of the ZnO NW array-based device with and without light illumination, indicating the Schottky contacts between the NWs and Ag electrodes. Schottky contacts should also play an important role in the high performance of ultra-violet photodetector. The Schottky barrier located at the contact areas can not

only accelerate the separation of photo-generated electron-hole pairs but also reduce the electron-hole recombination rate. Thus, it is beneficial to photocurrent and response speed[46-47]. As shown in Fig.4(b), the dark current is approximately 2.8 μA under a bias of 5 V and reaches approximately 29.5 μA under a bias of 5 V after light illumination. Fig.4(c) shows the *I*-*V* curves of ND-decorated ZnO NW-based PDs with and without light illumination. The dark current is approximately 55.2 μA, whereas the current could drastically increase to 327.9 μA once the UV illumination is on (Fig.4(d)), which is 16.5 times that of the bare ZnO device.

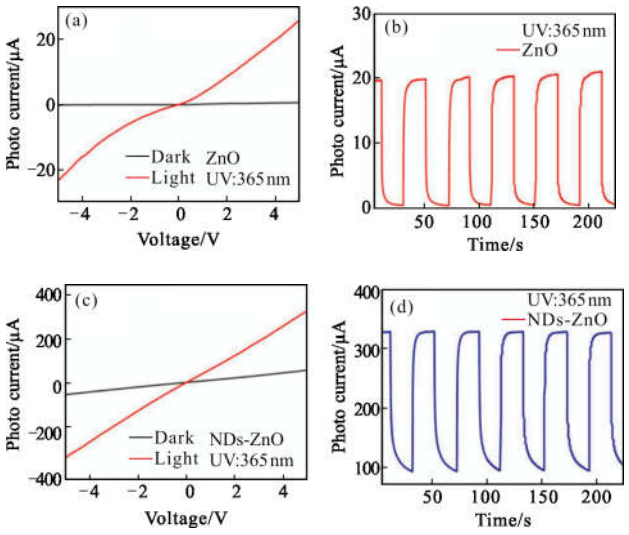

Fig.4 Photoresponse behavior of ZnO and ZnO-ND photodetectors with UV illumination (λ=365 nm, P= 14 mW/cm^2) under V_{ds}=5 V. (a) and (c) show *I*-*V* curves of ZnO NW and ZnO-NDs NWs with and without light illumination, respectively. (b) and (d) show *I*-*T* curves of ZnO NW and ZnO-ND NWs with 20 ms as sampling period under 5 V, respectively

1.5 Photodetection mechanism of ZnO-NDs

NDs can be introduced to improve the photodetector performance of the bare ZnO NWs UV PDs. Then, the mechanism on the photodetection perfor-mance enhancement of the hybrid ZnO-ND photodetector was investigated. Under illumination, the ZnO nanowires absorb photons with energy larger than that of the ZnO bandgap(E_{ph}>E_g) and generate a large number of electron-hole pairs according to the photoconductive effect[48]. Then, these photogenerated electron-hole pairs are separated and extracted by Ag electrodes in the op-posite directions under the applied electric field. This process generates photocurrent using the following equation:

$$I_{ph}=q\mu WEn\eta_{abs} \quad (1)$$

where μ is the carrier mobility, W is the channel width between the parallel electrodes, E is the applied electric field between electrodes, n is the excess carrier density, and η_{abs} is the material′s incident light absorption depth [48]. Therefore, the photocurrent is closely concerned with the excess carrier density (n) and the abilities of light harvesting (η_{abs}).

On the basis of XPS and PL results, the ZnO-NDs ultraviolet photodetection mechanism is schematically described in Fig.5. Under illumination with UV (365 nm), electron and hole pairs are excited in ZnO and NDs. The pairs in ZnO may be separated rapidly under the applied electric field, leading to its decent photodetection property. For the NDs, the small sp^2 C fraction on the NDs can drag the photoexcited carriers to the surface and then transfer to the ZnO nanowires due to the low energy levels for electron and hole in ZnO[44]. The photogenerated electrons in NDs can migrate more promptly to the ZnO nanowires than the photogenerated holes, leading to the rapid increase in excess carrier density in the ZnO nanowires. The phenomenon is called the synergistic effect between NDs and ZnO, mainly causing high-performance photodetection. In addition, the slow injecting holes result in the slow increase of the photocurrent, indicating slow time increase. The inconsistent migration rate of electrons and holes leads to excess electrons in ZnO and excess holes in NDs. That is, a portion of the photogenerated electron-hole pairs is spatially separated. When the light is turned off, the spatially unseparated electron-hole pairs rapidly recombine, leading to a quick decay of the photocurrent. On the contrary, the spatially separated electron-hole pairs cannot rapidly meet their

counterparts and recombine, thereby leading to the slow decay rate of the photocurrent.

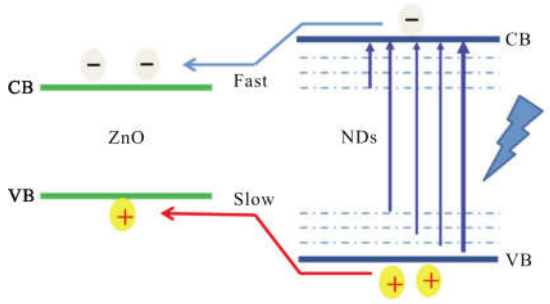

Fig.5 Electron-hole separation mechanism of the hybrid ZnO–NDs during light illumination

The isolated NDs (not attached on ZnO NWs) exhibit no photodetection performance. Photoexcited electrons and holes may recombine rapidly when the surface functional groups act as the PL centers because they localize at the surface of the NDs. Therefore, the synergistic effect of hybrid ZnO nanowires with nanodiamonds is crucial in the development of a highly sensitive photodetector.

2 Conclusion

Nanodiamond was introduced to improve the photodetection performance of ZnO for the first time. The prepared nanodiamond was mixed with a small sp^2 C fraction and formed a new bond with ZnO. Impressively, the photodetector based on ZnO–ND exhibits outstanding photodetection capabilities, which balance the high detectivity, fast response speed, and decent current on/off ratio simultaneously. The photodetector based on ZnO–ND is superior to the bare ZnO device and better than most of the reported nanomaterial-based photodetectors. Furthermore, a possible ND–mediated photodetection mechanism has been proposed. The excellent performance may be attributed to the synergistic effect between NDs and ZnO nanowires, greatly promoting the injection of photoexcited carriers from NDs to ZnO. These results suggest that NDs are promising for ameliorating the photodetection property of nanomaterials.

References:

[1] Patel M, Kim H, Kim J. All transparent metal oxide ultraviolet photodetector [J]. ***Advanced Electronic Materials***, 2016, 1(11): 1500232.

[2] Zhai T, Fang X, Liao M, et al. A comprehensive review of one-dimensional metal-oxide nanostructure photodetectors [J]. ***Sensors***, 2009, 9(8): 6504.

[3] Wang C, Yin L, Zhang L, et al. Metal oxide gas sensors: sensitivity and influencing factors [J]. ***Sensors***, 2010, 10(3): 2088.

[4] Liao X, Yan X, Lin P, et al. Enhanced performance of ZnO piezotronic pressure sensor through electron-tunneling modulation of MgO nanolayer [J]. ***Acs Appl Mater Interfaces***, 2015, 7(3): 1602–1607.

[5] Fulati A, Ali S M U, Riaz M, et al. Miniaturized pH sensors based on zinc oxide nano-tubes/nanorods [J]. ***Sensors***, 2009, 9(11): 8911–8923.

[6] Wan Q, Li Q H, Chen Y J, et al. Positive temperature coefficient resistance and humidity sens-ing properties of Cd–doped ZnO nanowires [J]. ***Applied Physics Letters***, 2004, 84(16): 3085–3087.

[7] Minami T. Transparent conducting oxide semiconductors for transparent electrodes [J]. ***Semi-conductor Science Technology***, 2005, 20(4): S35.

[8] Lang X, Hirata A, Fujita T, et al. Nanoporous metal/oxide hybrid electrodes for electrochemical supercapacitors [J]. ***Nature Nanotechnology***, 2011, 6(4): 232.

[9] Zhan Z Y, Xu C Y, Zhen L, et al. Large-scale synthesis of single-crystalline KNbO nanobelts via a simple molten salt method[J]. ***Ceramics International***, 2010, 36(2): 679–682.

[10] Zhan Z, An J, Zhang H, et al. Three-dimensional plasmonic photoanodes ba sed on Au-embedded TiO_2 structures for enhanced visible-light water splitting [J]. ***Acs Appl Mater Inter-Faces***, 2014, 6(2): 1139–1144.

[11] Kim K, Kim G, Lee B R, et al. High-resolution electro hydrodynamic jet printing of small-molecule organic light-emitting diodes[J]. ***Nanoscale***, 2015, 7(32):13410.

[12] Kim S Y, Kim K, Hwang Y H, et al. High-resolution electro hydrodynamic inkjet printing of stretchable metal oxide semiconductor transistors with high performance [J]. ***Nanoscale***, 2016, 39(8): 17113–17121.

[13] Kim M, Park J, Ji S, et al. Fully-integrated, bezel-less transistor arrays using reversibly foldable interconnects and

stretchable origami substrates [J]. ***Nanoscale***, 2016, 8(18): 9504-9510.

[14] Chen H, Liu H, Zhang Z, et al. Nanostructured photodetectors: from ultraviolet to terahertz [J]. ***Advanced Materials***, 2016, 28(3): 403.

[15] Tran V T, Wei Y, Yang H, et al. All-inkjet-printed flexible ZnO micro photodetector for a wearable UV monitoring device[J]. ***Nanotechnology***, 2017, 28(9): 095204.

[16] Zhan Z, An J, Wei Y, et al. Inkjet-printed optoelectronics[J]. ***Nanoscale***, 2016, 9(3): 965-993.

[17] Teng F, Zheng L, Hu K, et al. Surface oxide thin layer of copper nanowires enhanced UV selective response of ZnO film photodetector [J]. ***Journal of Materials Chemistry C***, 2016, 4(36): 02901A.

[18] Chen M, Hu L, Xu J, et al. ZnO hollow-sphere nanofilm-based high-performance and low-cost photodetector [J]. ***Small***, 2011, 7(17): 2449-2453.

[19] Galloro J, Ginzburg M, Míguez H, et al. Replicating the structure of a cross linked polyferrocenylsilane inverse opal in the form of a magnetic ceramic [J]. ***Advanced Functional Materials***, 2002, 12(5): 382-388.

[20] Retamal J R D, Chen C Y, Lien D H, et al. Concurrent improvement in photogain and speed of a metal oxide nanowire photodetector through enhancing surface band bending via incorporating a nanoscale heterojunction [J]. ***Acs Photonics***, 2014, 1(4): 354-359.

[21] Liu X, Gu L, Zhang Q, et al. All-printable band-edge modulated ZnO nanowire photodetectors with ultra-high detectivity[J]. ***Nature Communications***, 2014, 5(4007): 4007.

[22] Nasiri N, Bo R, Chen H, et al. Structural engineering of nano-grain boundaries for low-voltage UV -photodetectors with gigantic photo-to dark-current ratios [J]. ***Advanced Optical Materials***, 2016, 4(11): 1787-1795.

[23] Monroy E, Omnès F, Calle F. Wide-bandgap semiconductor ultraviolet photodetectors [J]. ***Semiconductor Science & Technology***, 2003, 18(4): R33.

[24] Fang X, Bando Y, Liao M, et al. Ultraviolet sensors: an efficient way to assemble ZnS nanobelts as ultraviolet-light sensors with enhanced photocurrent and stability [J]. ***Advanced Functional Materials***, 2010, 20(3): 500-508.

[25] Ding L, Liu N, Li L, et al. Graphene-skeleton heat-coordinated and nanoamorphous-surface-state controlled pseudo-negative-photoconductivity of tiny SnO_2 nano-particles [J]. ***Advanced Materials***, 2015, 27(23): 3525-3532.

[26] Li X, Gao C, Duan H, et al. High-performance photoelectrochemical-type self-powered UV photodetector using epitaxial TiO_2/SnO_2 branched heterojunction nanostructure[J]. ***Small***, 2013, 9(11): 2005.

[27] Xie Y, Wei L, Wei G, et al. A self-powered UV photodetector based on TiO_2 nanorod arrays [J]. ***Nanoscale Research Letters***, 2013, 8(1): 1-6.

[28] Fang X, Hu L, Huo K, et al. New ultraviolet photodetector based on individual Nb_2O_5 nanobelts [J]. ***Advanced Functional Materials***, 2011, 21(20): 3907-3915.

[29] Liu H, Zhang Z, Hu L, et al. New UV-A photodetector based on individual potassium niobate nanowires with high performance [J]. ***Advanced Optical Materials***, 2015, 2(8): 771-778.

[30] Zhou J, Gu Y, Hu Y, et al. Gigantic enhancement in response and reset time of ZnO UV nanosensor by utilizing Schottky contact and surface functionalization [J]. ***Applied Physics Letters***, 2009, 94(19): 191103.

[31] Cheng G, Wu X, Liu B, et al. ZnO nanowire Schottky barrier ultraviolet photodetector with high sensitivity and fast recovery speed [J]. ***Applied Physics Letters***, 2011, 99(20): 203105.

[32] Lu J, Xu C, Dai J, et al. Improved UV photoresponse of ZnO nanorod arrays by resonant coupling with surface plasmons of Al nanoparticles [J]. ***Nanoscale***, 2015, 7(8): 3396-3403.

[33] Fu X W, Liao Z M, Xu J, et al. Improvement of ultraviolet photoresponse of bent ZnO microwires by coupling piezoelectric and surface oxygen adsorption/desorption effects. [J]. ***Nanoscale***, 2013, 5(3): 916-920.

[34] He P, Feng S, Liu S, et al. Ultrafast UV response detectors based on multi-channel ZnO nan-owire networks [J]. ***Rsc Advances***, 2015, 5(127): 105288-105291.

[35] Liu J, Lu R, Xu G, et al. Development of a seedless floating growth process in solution for synthesis of crystalline ZnO micro/nanowire arrays on graphene: towards high-performance nanohybrid ultraviolet photodetectors [J]. ***Advanced Functional Materials***, 2013, 23(39): 4941-4948.

[36] Zhan Z, An J, Zhang H, et al. Three-dimensional plasmonic photoanodes based on Au-embedded TiO_2 structures for enhanced visible-light water splitting [J]. ***Acs Appl Mater Interfaces***, 2014, 6(2): 1139-1144.

[37] Liu K, Sakurai M, Liao M, et al. Giant improvement of the performance of ZnO nanowire photodetectors by Au nanoparticles [J]. ***Journal of Physical Chemistry C***, 2010, 114(114): 19835-19839.

[38] Zhan Z, Liu L, Wang W, et al. Ultrahigh surface-enhanced raman scattering of graphene from Au/Graphene/Au sandwiched structures with subnanometer gap [J]. ***Advanced Optical Materials***, 2016, 4(12): 2021-2027.

[39] Nasiri N, Bo R, Fu L, et al. Three-dimensional nano-heterojunction networks: a highly per-forming structure for fast visible-blind UV photodetectors [J]. ***Nanoscale***, 2017, 9 (5): 2059.

[40] Chen C Y, Chen M W, Hsu C Y, et al. Enhanced recovery speed of nanostructured ZnO photodetectors using nanobelt networks [J]. ***IEEE Journal of Selected Topics in Quantum Electronics***, 2012, 18(6): 1807-1811.

[41] Zheng Q, Huang J, Yang H, et al. A high-performance nanobridged MoO_3 UV photodetector based on nanojunctions with switching characteristics [J]. ***Nanotechnology***, 2017, 28 (4): 045202.

[42] Huang M H, Wu Y, Feick H, et al. Catalytic growth of zinc oxide nanowires by vapor transport [J]. ***Advanced Materials***, 2001, 13(2): 113-116.

[43] Sankaran K J, Kalpataru P, Balakrishnan S, et al. Catalytically induced nanographitic phase by a plati-num-ion implantation/ annealing process to improve the field electron emission properties of ultrananocrystalline diamond films [J]. ***J Mater Chem C***, 2015, 3(11): 2632-2641.

[44] Lin Z, Xiao J, Li L, et al. Nanodiamond-embedded p-type copper (I) oxide nanocrystals for broad-spectrum photocatalytic hydrogen evolution [J]. ***Adv Energy Mater***, 2016, 6: 1501865.

[45] Xiao J, Liu P, Li L, et al. Fluorescence origin of nanodiamonds[J]. ***J Phys Chem C***, 2015, 119(4): 2239-2248.

[46] Zhou X, Gan L, Tian W, et al. Ultrathin $SnSe_2$ flakes grown by chemical vapor deposition for high-performance photodetectors[J]. ***Adv Mater***, 2015, 27(48): 8035-8041.

[47] Hu X, Zhang X, Liang L, Bao J, et al. High-performance flexible broadband photodetector based on organo lead halide perovskite[J]. ***Adv Funct Mater***, 2014, 24 (46): 7373-7380.

[48] Island J O, Blanter S I, Buscema M, et al. Gate controlled photocurrent generation mechanisms in high-gain In_2Se_3 phototransistors [J]. ***Nano Letters***, 2015, 15 (12): 7853-7858.